Simultaneous description of elastic, fusion and total reaction cross sections for the $^6He +^{209} Bi$ system for energies around the coulomb barrier

A. Gómez Camacho and E.F. Aguilera

Departamento del Acelerador, Instituto Nacional de Investigaciones Nucleares,
Apartado Postal 18-1027, 11801, México, D.F.

A systematic and simultaneous description of elastic scattering, reaction and fusion cross sections for the system $^6He +^{209} Bi$ at energies below the Coulomb barrier is given within the direct reaction theory. Woods-Saxon optical potentials are used in the calculations where a cut-off parameter R_F is defined to separate the fusion and direct reaction absorption processes. A χ^2-search for energy dependent forms for the diffuseness parameter a_I and the radial parameter R_I of the imaginary potential W_α that best fits the experimental data is carried out. Good fits to the data are found. A relationship between the large values found for a_I and R_I with the large spatial extension of the halo nucleus ^6He wave function is also looked for.

Keywords: Nuclear reactions; exotic nuclei; nuclear fusion.

Se ha hecho un estudio simultáneo y sistemático de las secciones eficaces de dispersión elástica, reacción total y de fusión para el sistema nuclear $^6He +^{209} Bi$ para energías alrededor de la barrera Coulombiana. En el estudio se utiliza un potencial de Woods-Saxon para el que se define un parámetro de corte R_F para dividir el proceso de absorción correspondiente a fusión del de reacciones directas. Igualmente se realizan ajustes χ^2 para encontrar los mejores ajustes a los datos experimentales mediante relaciones dependientes de la energía para los parámetros a_I y R_I de la parte imaginaria W_α del potencial óptico. Los resultados para todas las secciones eficaces concuerdan en buena medida con los datos experimentales. Finalmente se trata de determinar una relación entre los valores relativamente grandes de a_I y R_I con el extenso halo del nucleo ^6He.

Descriptores: Reacciones nucleares; núcleos exóticos; fusión nuclear.

PACS: 25.60Bx; 25.60.Dz; 25.60.Pj; 24.10.Ht

1. Introduction

In a recent work, exceptionally anomalous strong reaction cross sections were found in the interaction of the "Borromean" nucleus ^6He with a ^{209}Bi target at energies around the Coulomb barrier [1]. Strong anomalous breakup/transfer-yields were obtained in the $^{209}Bi(^6He,^4 He)$ reaction, and consequently large reaction cross sections were derived from the $^{209}Bi(^6He,^6 He)$ elastic scattering data measured in the same work [1, 2]. Enhanced fusion excitation functions were also measured for the same system [3]. The total reaction cross section was simply determined by the sum of the fusion and breakup-transfer yields. In the calculations of Ref. 2, two different optical model descriptions were given that use energy dependent absorptive optical potentials which match the elastic and total reaction data equally well. In one of the descriptions the Woods-Saxon absorptive potential becomes more diffuse at lower energies while the other uses a folding model [4], and involves an increasing radius for the imaginary well at lower energies. However, although scattering angular distributions and total reaction excitation functions have been well predicted by both of these descriptions, no account for fusion has been given within the same description. It is the purpose of the present work to show that it is possible to give a simultaneous description of the elastic scattering, fusion and total reaction cross section experimental data for the reaction $^6He +^{209} Bi$ at the measured energies; 14.3, 15.8, 17.3, 18.6 and 21.4 MeV. The approach to be used here will be consistent with the direct reaction theory

which means that at every step of the calculations the optical potentials to be used must be such that elastic scattering is well described. In other words, the description of the fusion and reaction processes is given in such a way that it is consistent with the observed elastic scattering. The basic concept of the approach is to define a Woods-Saxon potential U whose absorptive component W_α (α being the elastic channel) is split into two parts, one responsible for only the fusion absorption process, and the other for the rest of the reaction processes. We call these two parts the fusion part W_F and the direct reaction part W_{DR} respectively. The fusion cross section σ_F can be obtained from that portion of the total reaction cross section due solely to W_F. On the other hand, the direct reaction cross section is given in terms of W_{DR}. Since the total absorption potential which is used in the elastic scattering calculation will remain itself unmodified, the fusion is calculated in consistency with the elastic scattering, and total reaction cross section calculations. In our approach the diffuseness parameter a_I and the radial parameter R_I of the absorptive part W_α of the Woods-Saxon optical potential will be determined by a χ^2-analysis of the elastic scattering, and total reaction experimental data. The fusion cut-off parameter that splits W_α into a fusion part and a direct reaction part is calculated in conjunction with a_I and R_I [5–7]. As a first calculation, we determine the best energy dependent equations for a_I and R_I that fit the elastic and total reaction data alone. Then, the best energy dependent fit for R_F is found. Next a simultaneous determination of a_I, R_I and R_F is done, and the results are compared with the foregoing cal-

culation. Throughout the calculations a relationship between the large values for the diffuseness and radial parameters a_I and R_I with the expected large radial spatial extension of the halo nucleus ^6He is discussed. So, it is attempted to find out how the halo structure of ^6He might intervene in the absorption processes.

In Sec. 2, a brief description of our method is presented. In Sec. 3, the results of the calculations are shown. Finally, in Sec. 4, a summary and a discussion is given.

2. Brief theoretical description

Possibly the simplest choice for the fusion potential W_F is to make it equal to the absorptive imaginary part W of the Woods-Saxon potential U for radial distances r shorter than some R_F, and zero for larger distances than R_F. That is,

$$W_F(r) = \begin{cases} W(r) & r \le R_F \\ 0 & r \ge R_F \end{cases} \qquad (1)$$

where $R_F = r_F(A_1^{1/3} + A_2^{1/3})$, r_F being the fusion radius parameter which will be determined phenomenologically. Of course W_{DR} is defined accordingly as $W_{DR}(r) = 0$ for $r \le R_F$, and $W_{DR}(r) = W(r)$ for $r \ge R_F$. Basically the formalism begins with the Schrödinger equation for elastic scattering from an optical potential,

$$(T_\alpha + U_\alpha)\chi_\alpha^{(+)} = E_\alpha \chi_\alpha^{(+)}, \qquad (2)$$

where α is the elastic incident channel, $U_\alpha = V_\alpha - iW_\alpha$ is the elastic optical potential and $\chi_\alpha^{(+)}$ is the distorted wave function. The real and imaginary parts of the optical potential U_α are assumed to be of the Woods-Saxon form, that is,

$$V_\alpha(r) = \frac{V_{0,\alpha}}{1 + \exp(\frac{r-R_V}{a_V})}, \qquad (3)$$

and

$$W_\alpha(r) = \frac{W_{0,\alpha}}{1 + \exp(\frac{r-R_I}{a_I})}. \qquad (4)$$

As it is well known, the total reaction cross section can be calculated by

$$\sigma_R = \frac{2}{\hbar v_\alpha} \left\langle \chi_\alpha^{(+)} \left| W_\alpha \right| \chi_\alpha^{(+)} \right\rangle, \qquad (5)$$

where v_a is the relative velocity between projectile and target. The fusion cross section is similarly calculated by,

$$\sigma_F = \frac{2}{\hbar v_\alpha} \left\langle \chi_\alpha^{(+)} \left| W_{F,\alpha} \right| \chi_\alpha^{(+)} \right\rangle, \qquad (6)$$

where $W_{F,\alpha}$ is defined by Eq.(1). It is important to point out that the distorted wave function that appears in Eq.(6) is the same as that in Eq.(5), and is the solution of Eq.(2). We call σ_F the fusion cross section that proceeds through the elastic channel α or in short the elastic fusion cross section. In this

sense we say that our fusion cross section calculation is consistent with the elastic scattering. Integrating Eq.(6) over the angles, we have

$$\sigma_F = \frac{\pi}{k_\alpha^2} \sum_{l_\alpha} (2l_\alpha + 1) \frac{8}{\hbar v_\alpha} \int \left| \chi_\alpha^{(+)}(r) \right|^2 W_{F,\alpha}(r) dr. \quad (7)$$

Evidently the corresponding direct reaction cross section has a similar expression to the last equation except that $W_{F,\alpha}(r)$ is substituted by $W_{DR,\alpha}(r)$. Throughout the calculations only coupling to the elastic channel was considered, that is fusion going first through excited states of the colliding nuclei was ignored. We will see that this assumption becomes good enough to give a good description to the experimental data.

3. Numerical Calculations

In this section the calculations of elastic, fusion, and total reaction cross section calculations are presented for the system $^6\text{He}+^{209}\text{Bi}$ at the center of mass energies 14.3, 15.8, 17.3, 18.6, and 21.4 MeV. It is important to emphasize that the fusion cross section will be calculated simultaneously with elastic scattering and total reaction cross sections by introducing a cut-off parameter r_F that will divide the optical potential into a fusion part, and a direct reaction part. In a first calculation the only Woods-Saxon optical potential parameter that will vary with the incident energy is the imaginary diffuseness parameter, the other parameters will remain constant as shown in the upper part of Table I. A χ^2-analysis of elastic scattering data is now executed where good fits are obtained for minimum values of the reduced $\chi_\nu^2 = \chi^2/\nu$, defined as,

$$\chi_\nu^2 = \frac{1}{\nu} \sum_{i=1}^{N} \left\{ \frac{1}{\sigma_i^2} \left[y_i - y(x_i) \right]^2 \right\} \qquad (8)$$

where ν is the number of degrees of freedom for a function $y(x_i)$ with n parameters. That is, the number of degrees of freedom is given by, $\nu = N - n - 1$, N being the number of data points, and σ_i is their uncertainty. Then, allowing only the diffuseness a_I to vary, best fits to the data gave the following values of χ_ν^2; 4.67, 0.99, 0.52, 0.75, and 1.5 for the center of mass energies 14.3, 15.8, 17.3, 18.6, and 21.4 MeV respectively. We found that the determined values for a_I follow the linear equation,

$$a_I = (1.964 - 0.045 E_{cm}) \text{ fm} \qquad (9)$$

Now, the fusion radius parameter R_F of Eq.(1) will be determined so as to fit the fusion data of Ref. [3]. By using Eq.(9), we found that the fusion data can be well described if the fusion cut-off parameter R_F follows the linear parametrization,

$$R_F = (14.4 - 0.0984 E_{cm}) \text{ fm}. \qquad (10)$$

The calculated elastic scattering cross section is shown in Fig. 1(full lines) compared to the data for all the energies. The results for the total reaction and fusion cross sections are shown by the full lines of Figs. 2 and 3 respectively. As seen, the fusion cross section is well described by our calculation, and the reaction cross section is possibly a little underpredicted for 14.3, 17.3, and 21.4 MeV. Of course the values taken by R_F does not influence the calculation of the total reaction σ_R. However, it is important to emphasize once more that in this calculation we do not vary any parameter other than R_F and a_I, which vary according to Eqs. (9) and (10), all the other optical potential parameters have kept fixed.
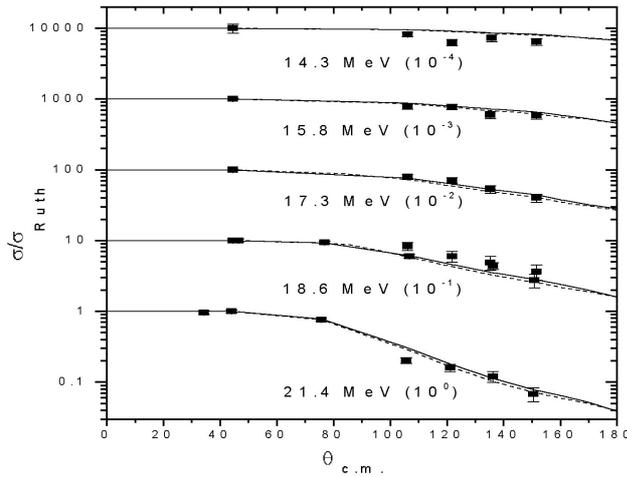

FIGURE 1. Calculated angular elastic scattering cross section distribution following Eq.(9) (solid-line) and Eq.(11) (dashed-line). Experimental data corresponds to Ref. 2.
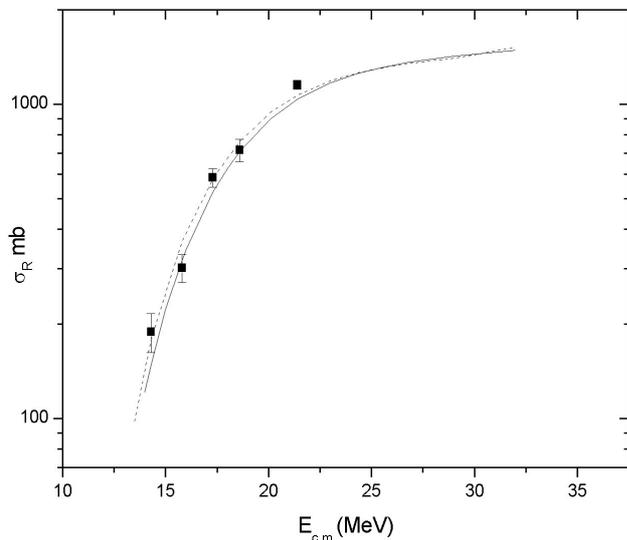

FIGURE 2. Total reaction cross section corresponding to a Woods-Saxon parametrization with a diffuseness given by Eq.(9) (solid-line) and by Eq.(11) (dashed-line). Experimental data corresponds to Ref. 2.
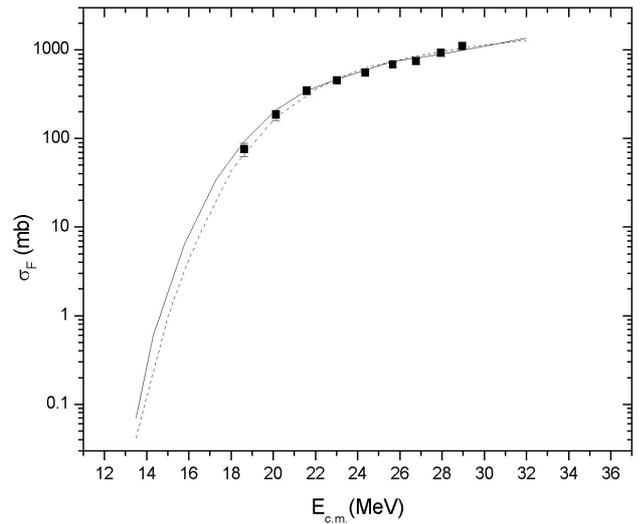

FIGURE 3. Simultaneous fusion cross section calculation based on a cut-off fusion radius parametrization following Eq.(10) (solid-line) and Eq.(12) (dashed-line). Experimental data are taken from Ref. 1.

Now, in order to improve the calculation particularly that of σ_R, instead of following the recipe of Eq.(9), we have allowed our computer program to find by itself the best values of the diffuseness parameter a_I of W_α, and of the cut-off parameter R_F simultaneously. In this way both the total reaction and fusion cross section are fitted simultaneously. The new calculation shows that the fit to the elastic scattering, and the total reaction cross section can be further improved if the following formula is used,

$$a_I = 2.060 - 0.0488 E_{cm} \text{ fm.} \qquad (11)$$

As before, the fusion cross section fitting to the data produces slightly scattered values for R_F, but a linear least squares fit to these scattered values is used in a final calculation of σ_F. That is given by the equation,

$$R_F = 15.498 - 0.147 E_{cm} \text{ fm.} \qquad (12)$$

The final results obtained by using the last two equations while keeping all the other potential parameters the same as before, are shown by the dashed lines of Figs. 1, 2, and 3. As seen in these figures, the elastic scattering, and fusion cross sections are also well described, but particularly the reaction cross section is now closer to the data than in the foregoing calculation.

In a second calculation, instead of varying the diffuseness parameter a_I of the absorption potential W_α, the radial parameter R_I is allowed to change. The real and imaginary potential strengths used in this second calculation are determined as in the folding potential calculation of Mohr [8]. That is, the strength W_α of the imaginary potential is obtained by the volume integral,

$$J_I(E) = \frac{4\pi}{A_p A_t} \int_0^\infty W_\alpha(r, E) r^2 dr, \qquad (13)$$

TABLE I. Optical potential parameters used in the calculations. All potential depths and the center of mass energies are in MeV. Radial and diffuseness parameters in fm.

a_I and r_F are varied.	$V_{0,\alpha}$	r_V	a_V	$W_{0,\alpha}$	r_I	a_I
For all energies	150.0	1.02	0.68	25.0	1.2	Eq.(11)
r_I and r_F are varied						
14.3	118.43	1.2	0.68	2.29	Eq.(19)	0.6
15.6	119.37	1.2	0.68	3.77		0.6
17.3	120.24	1.2	0.68	5.89		0.6
18.6	120.91	1.2	0.68	8.34		0.6
21.4	122.12	1.2	0.68	15.75		0.6

and the real part V_α by a similar equation. The energy dependence of the volume integral J is given by the parametrization of Ref. 9 i.e.,

$$J_{R,I}(E_{cm}) = J_{R,I}^0 \exp[-(E_{cm} - E_{R,I}^0)^2/\triangle_{R,I}^2], \quad (14)$$

with the following parameters,

$$J_R^0 = 350 \text{ MeV}, E_R^0 = 30 \text{ MeV and } \triangle_R = 75 \text{ MeV}, \quad (15)$$

while for the absorption part,

$$J_I^0 = 127 \text{ MeV}, E_I^0 = 30 \text{ MeV and } \triangle_I = 12.7 \text{ MeV}. \quad (16)$$

Woods-Saxon shapes are assumed for both potentials where for each center of mass energy, the depth of the real and imaginary parts are determined by Eqs.(13)-(16). The values so determined are shown in the lower part of Table I.

With these potential parameters, an χ_ν^2−search of elastic and total reaction cross section data give a best fit when the radial parameter R_I of the absorption potential is varied according to the equation,

$$R_I = (5.314 + 131.7/E_{cm}) \text{ fm.} \quad (17)$$

The elastic scattering results are shown by the full lines of Fig. 4, which are very close to those of Ref. 8. The calculated total reaction cross section is shown by the full line of Fig. 5 in comparison to the data of Ref. 2. It can be said that our calculation for σ_R is basically under the expected values mainly in the low energy region. We now proceed to find the best fitting to the fusion cross section data. It was found that the fit to the experimental fusion data at the center of mass energies 14.3, 15.8, 17.3, 18.6, and 21.4 MeV produced scattered values for the cut-off parameter that can be adjusted by the straight line,

$$R_F = (14.82 - 0.126E_{cm}) \text{ fm.} \quad (18)$$

The calculated σ_F, obtained with this equation for R_F, is presented by the full line of Fig. 6 in comparison with the data of Ref. 1. In this case the fusion cross section is basically above the expected values. As done before, and in order to improve the predictions for the total absorption and

fusion cross sections, now we allow our program to simultaneously determine by itself the best R_I and R_F parameters for each center of mass energy. Keeping all the other parameters fixed as above, we find that the best R_I values are slightly dispersed around the straight line

$$R_I = (3.65 + 166.15/E_{cm}), \quad (19)$$

and the fit to the fusion data gives scattered values for the fusion parameter R_F which can be well described by the linear expression

$$R_F = (16.30 - 0.199E_{cm}) \quad (20)$$

The results for elastic, total reaction and fusion excitation functions with the use of Eqs. (19), and (20) are shown by the dashed lines of Figs. 4, 5, and 6 respectively. Now the fusion excitation function has become closer to the experimental data particularly in the high energy region. The total reaction cross section calculation has been greatly enhanced for low energies being also much closer to the data.
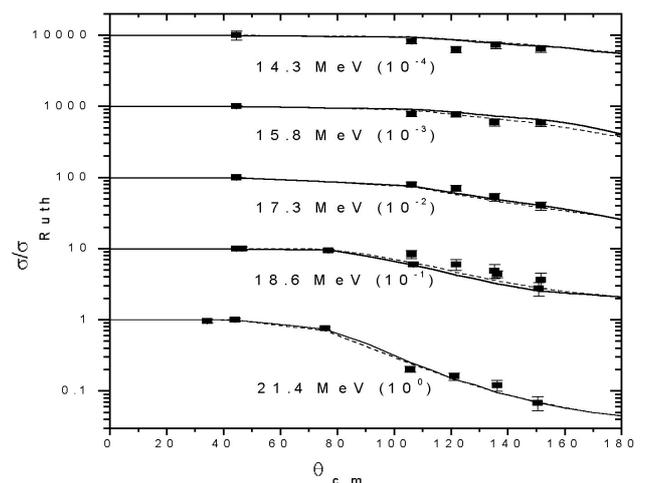

FIGURE 4. Angular elastic scattering cross section distribution calculated with Eq.(17) (solid-line) and with Eq.(19) (dashed-line). See text for details. Experimental data corresponds to Ref. 2.
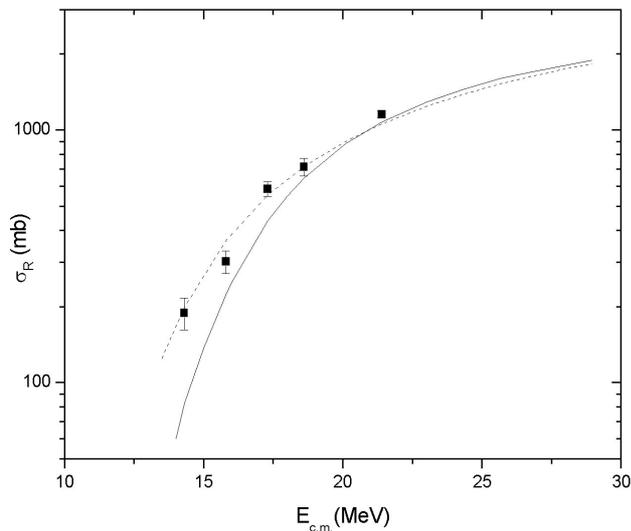
FIGURE 5. Total reaction cross section corresponding to a Woods-Saxon parametrization with a radial parameter given by Eq. (17) (solid-line) and by Eq. (19) (dashed-line). Experimental data corresponds to Ref. 2.
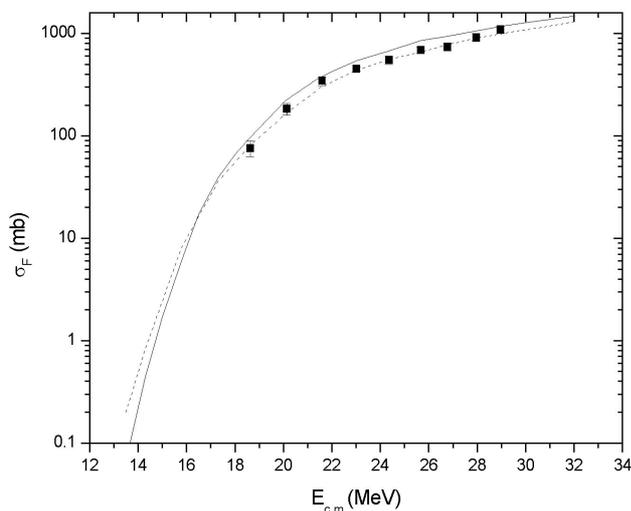

FIGURE 6. Simultaneous fusion cross section calculation based on a cut-off fusion radius parametrization following Eq. (18) (solid-line) and Eq. (20) (dashed-line). Experimental data are taken from Ref. 1.

Certainly one may question the significance of an χ_ν^2−analysis for a small number of angular elastic scattering data points (five for each energy). However, in the end only two parameters in Eqs. (9) and (10) are determined out of five angular distributions containing a total of 32 points (*i.e.* 30 degrees of freedom). Even in the intermediate χ_ν^2-fits of individual angular distributions, which should be thought only as a guide, the corresponding χ_ν^2 distribution for 4 degrees of freedom gives reasonable probability values for most angular distributions. At the very end, after including the total cross section and fusion data points, only four parameters will be calculated [Eqs. (11) and (12), or (19) and (20)] out of 46 experimental points, that is a total 42 degrees of freedom. Because of the inherent numerical complexity of optical model calculations, an iterative χ_ν^2−analysis starting with single angular distributions, but gradually involving more data points is done in one single calculation.

Therefore, we can conclude this section by establishing that in our approach, the elastic scattering, total reaction and fusion cross sections give closer results to the data when they are calculated simultaneously. A detailed discussion of the results as well as a search for a relationship between the optical potential parameters a_I and R_I with the expected large radial extension of the wave function of the halo nucleus ^6He will be given in the next section.

4. Summary and discussion

In this work, we have presented an approach to simultaneously calculate the elastic, reaction, and fusion cross sections. The method has been applied to the interaction between the halo nucleus ^6He and a ^{209}Bi target at the center of mass energies close to the Coulomb barrier energy. The basic idea of the method consists in defining a fusion cut-off radius parameter R_F for which all the incident-channel absorption goes to fusion for radial distances lower than R_F, and to direct reaction processes alone for distances bigger than R_F. Woods-Saxon potentials have been used in the calculations whose absorption part W_α is energy dependent through the diffuseness a_I or radial R_I parameters. A thorough analysis of the effect of this absorption potential energy dependence on the elastic, reaction, and fusion cross sections has been performed. For all the bombarding energies, fitting to the fusion experimental data has been achieved by a linear energy dependent expression for the fusion radius parameter R_F. We first allowed the diffuseness parameter a_I of W_α to be determined in the χ_ν^2−analysis of the elastic and total reaction experimental data. The best fitting to the data that minimizes the reduced χ_ν^2 has been achieved when a_I is described by Eq. (9). Then, we proceed to fit the fusion experimental data which was well described by the use of a linear relation for the fusion cut-off parameter R_F of Eq. (10). At this point, the overall theoretical results of elastic, reaction, and fusion cross sections were in good accordance with the data, however some deviations still existed. A more precise calculation was then searched but instead of following Eq. (9), we allowed a_I to be calculated in consistence with R_F, that is both parameters were calculated simultaneously in the χ_ν^2−analysis. This has given us Eqs. (11) and (12) and the resulting calculations for reaction, and fusion cross sections have been improved. Particularly, the reaction cross section became closer to the data. This can be explained from the fact that the absorption potential is now more diffuse particularly for low energies, and there can be more absorption for larger radial distances as can be seen in Fig. 7a.

Then we proceeded to perform a calculation in which the imaginary part of the Woods-Saxon potential is now energy dependent through the radial parameter R_I. As done before, first it was attempted to find a simultaneous description of the elastic and reaction excitation functions. Good fits to the data
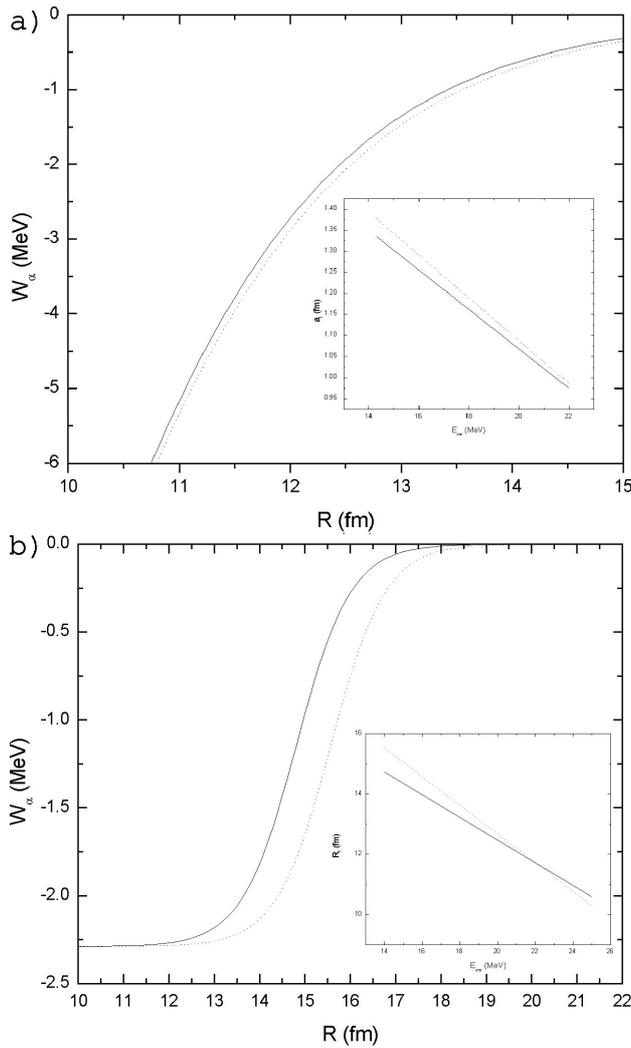
FIGURE 7. a) Imaginary optical potential W_α as function of $R_I = r_I(A_1^{1/3} + A_2^{1/3})$ for 14.3 MeV when its diffuseness is given by Eqs. (9) and (11). In the inset, the diffuseness of Eqs. (9) and (11) as function of the center of mass energy; b) Imaginary optical potential W_α as function of $R_I = r_I(A_1^{1/3} + A_2^{1/3})$ for 14.3 MeV when its radial parameter is given by Eqs. (17) and (19). In the inset, Eqs. (17) and (19) as function of the center of mass energy.

were obtained through the use of Eq. (17). However, the calculated total reaction cross section resulted under the expected values especially for low energies. Then, we proceeded to fit the fusion cross section which was correctly calculated by the Eq. (18). Next, we allowed R_I to be determined in consistency with R_F for each energy, the resulting Eqs. (19) and (20) were obtained from the best simultaneous fit to all the data. Fig.7b illustrates the increasing range of absorption when using Eq. (19).

It is very interesting to notice that the values taken by R_F of Eq. (12) lie in the range from 13.29 fm to 12.26 fm for energies between 15 MeV and 22 MeV. These R_F values are well above the contact parameter given by $R_m = R(^6He) + R(^{209}Bi)$. That is, since the nu-

clear matter mean-square radius $R_{m,rms}$ for ^6He is about 2.73 fm [10], then $R_m = 2.73 + 1.2A_{Bi}^{1/3} = 9.85$ fm. Now if the $^6He-$neutron matter distribution radius is used instead, that is $R_{rms}^n = 2.87$ fm [10] then $R_m = 9.99$ fm. These values suggest that in the fusion reaction of ^{209}Bi with the halo nucleus ^6He a very strong neck-formation effect might take place [11]. A possible explanation for this strong effect may be found in the large spatial extension of the ^6He-wave function. The decreasing R_F values with increasing energy indicates that as the incident energy becomes higher the length of the fusion neck becomes smaller. On the other hand, the fact that the diffuseness parameter a_I of the imaginary absorption potential W_α takes values anomalously large in the range of energies of interest (1.377 fm for 14 MeV to 0.84 fm for 25 MeV) can be empirically related to the large neutron halo radial distribution of ^6He. For the halo nucleus ^6He, we may expect that the description of its internal state function, in particular the nuclear halo by a Woods-Saxon well be related to a large diffuseness parameter. In Table I, we show how the R_{rms} varies with the diffuseness parameter. We have used optical potential parameters that correctly reproduce the 2-neutron-$p_{3/2}$ binding energy (0.96 MeV). The best value for the diffuseness parameter that reproduce the experimental $R_{rms}^n=2.87$ fm [10] is $a = 0.75$ fm. This fact shows that the nuclear surface or extended halo for ^6He can be simulated by a large diffuseness. It is important to emphasize that our direct reaction approach to fusion can not take into consideration the explicit influence of the two-neutron halo structure of ^6He on the reaction and fusion processes. The only way in which we can account for the effect of the neutron halo is through its contribution to the relative motion distorted wave function $\chi_\alpha^{(+)}$ for which anomalous large values of the diffuseness parameter a_I of the absorptive Woods-Saxon potential have been found.

Going back to the calculated fusion excitation functions obtained with R_F given by Eqs. (12) and (20) (dashed-lines of Figs. 3 and 6). These two equations were obtained for best fits to the data when a_I and R_F or alternatively R_I and R_F were determined simultaneously. Both calculations give a good description of the data ($\chi_\nu^2 = 0.9$ and 0.8, respectively). Since the values taken by R_F in the energy region of interest are similar for both cases, one might ask whether a good description can be given by a single formula for R_F as well. After weighing the contributions of Eqs. (12) and (20), the following formula for the radial cut-off parameter is found,

$$R_F = 15.982 - 0.177E_{cm} \text{ fm} \qquad (21)$$

which gives a fairly good account for the fusion data for both cases ($\chi^2 = 5.2$).

We conclude this discussion by making some comments about the role of the halo of ^6He when interacts with ^{209}Bi. It has been suggested above that the nuclear halo of the nucleus ^6He can be implicitly considered through a large diffuseness or a large radial parameter of the relative Woods-Saxon potential. We intend in this last part to make this sug-

TABLE II. Relationship between diffuseness a and radius R of an optical potential to the neutron mean square radius R_{rms}^n. In all cases the proton potential depth is fixed to $V_p = -58.5$ MeV. All the potentials sets reproduce the experimental neutron-$p_{3/2}$ bound energy of 0.96 MeV

V_n MeV	a fm	R_{rms}^n fm	V_n MeV	R fm	R_{rms}^n fm
-58.7	0.55	2.609	-58.7	2.0	2.609
-56.0	0.65	2.75	-50.7	2.18	2.696
-53.3	0.75	2.88	-44.3	2.36	2.77
-46.1	1.0	3.22	-39.0	2.55	2.86

gestion clearer. For that purpose two calculations are performed for the neutron internal wave function ϕ^n, and neutron root–mean-square radius R_{rms}^n with a Woods-Saxon potential well of; i) variable diffuseness a and ii) variable radial parameter R. In all the calculations the experimental two-neutron binding is fitted by adjusting the depth of the potential. It can be seen in Table II, that the large experimental value for R_{rms}^n of ^6He can be simulated either by a large diffuseness parameter or a large radial parameter R of a Woods-Saxon potential. In fact the experimental R_{rms}^n=2.87 fm is obtained when $a = 0.75$ fm, $R = 2.0$ fm, $V_n = -53.3$ MeV and when $R = 2.55$ fm, $a = 0.55$ fm, $V = -39.0$. Therefore, the extended neutron halo of ^6He must play an important role in the interaction with ^{209}Bi since nuclear reactions can begin at larger distances, and this fact is also represented by the large values of the diffuseness or the radial parameters of the absorptive potential W_α.

Finally, it is remarkable that we can get simultaneous good fits to all the data in both cases (see Table I) in spite of the fact that the optical potential parameters are quite dif-ferent. It is true that for the class of nuclear reactions that we have tried to study for the $^6He +^{209} Bi$ system with the use of an optical potential model, the values of the geometrical parameters of the Woods-Saxon potential such as the diffuse-ness and reduced radial distance are more important than the central values of the potential depths. This is so, since these geometrical parameters greatly determine the interaction at the surface of the colliding nuclei than in the inner region where the potential depths are more important. However, it is interesting to notice that in the first calculation where the dif-fuseness a_I of W_α and fusion cut-off radius R_F were varied, the real potential depth V_α remained fixed at 150 MeV. In the second case, where the reduced radial parameter R_I and R_F were varied, the depth varied between 118 and 122 MeV. On the other hand, the imaginary part being constant in the first case varies very strongly in the second. Clearly, even though the results of the calculations and the agreement with the data are more influenced by the large values of the diffuseness a_I and of the reduced radial R_I parameters in the peripheral re-gion, it is true that the different behavior of W_α and V_α as well as of a_I and R_I in both calculations must combine to produce distorted wave functions $\chi_\alpha^{(+)}$ that compensate for the differences so that when used in Eq. (6), reproduce a to-tal reaction cross section that fit the experimental data. It is nice to see that once the distorted wave function $\chi_\alpha^{(+)}$ has been determined with the above mentioned variations, the fu-sion potential $W_{F,\alpha}$ as defined by the cut-off parameter R_F is such that the predictions of Eq. (7) agree very well with the data.

Acknowledgments

1. E.F. Aguilera *et al.*, *Phys. Rev. Lett.* **84** (2000) 5058.

2. E.F. Aguilera *et al.*, *Phys. Rev.* **C63** (2001) 061603(R).

3. J.J. Kolata *et al.*, *Phys. Rev. Lett.* **81** (1998) 4580.

4. G.R. Satchler and W.G. Love, *Phys. Rep.* **55** (1979) 183.

5. T. Udagawa, B.T. Kim, and T. Tamura, *Phys. Rev. C* **32** (1985) 124.

6. T. Udagawa and T. Tamura, *Phys. Rev. C* **29** (1984) 1922.

7. A. Gómez Camacho and T. Udagawa, *Rev. Mex. Fís.* **44** (1998) 85.

8. P. Mohr, *Phys. Rev. C* **62** (2000) 061601(R).

9. P. Mohr, *Phys. Rev. C* **61** (2000) 045802.

10. O. Tanihata *et.al. Phys. Rev. Lett.* **55** (1985) 2676.

11. C.E.Aguiar, V.C.Barbosa, L.F. Canto, and R. Donangelo, *Phys. Lett. B* **201** (1988) 22.